Two-Dimensional Flexural-Gravity Waves of Finite Amplitude in Deep Water

Z. Wang[1], J.-M. Vanden-Broeck[1] & P. A. Milewski[2]

[1]*Department of Mathematics, University College London, London, WC1E 6BT*

[2]*Department of Mathematical Sciences, University of Bath, Bath, BA2 7AY*

Steady periodic and solitary waves propagating in a two-dimensional fluid bounded above by a flexible sheet - which may be viewed as modeling an ice sheet - are considered in deep water. The nonlinear elastic model is based on the special Cosserat theory of hyperelastic shells proposed by Toland (2008) for this problem. Numerical solutions are computed via conformal mapping and a pseudo-spectral method. New solitary waves are found by using a continuation method to follow the branch of elevation waves. The results extend Guyenne and Părău's findings (Guyenne & Părău (2012)). It is shown that, for periodic waves, far along the branches the profiles become overhanging and ultimately approach configurations with a trapped bubble at their troughs.

Keywords: flexural-gravity, elevation branch, overhanging waves

1. Introduction

The flexural-gravity (FG) wave problem is concerned with deformations of a thin elastic sheet on the surface of a fluid as it responds to and generates hydrodynamic excitation. Both bending and gravity act as restoring forces. FG wave theory can be applied in offshore and polar engineering in the study of large floating structures (such as floating runways) or to understand the response of floating ice sheets, either used as runways or roads or responding to oceanic waves. FG waves are often generated by moving loads such as vehicles or a landing aircraft. Large-amplitude deflections of the ice sheets, including fully localized structures (Wilson (1958)) and periodic waves (Hegarty & Squire (2002)), have been observed in the experiments. In order to understand forced responses, it is crucial to know the free response of the system, such as periodic and solitary waves. These will be considered in the highly nonlinear regime in this paper.

For simplicity we assume that the flow is two-dimensional, inviscid and irrotational. The large floating structure or ice sheet resting on the top of the fluid is modeled as a thin elastic plate responding to bending forces, while its inertia and forces due to stretching are neglected. For the ice sheet problem, this is a reasonable approximation. The pressure jump exerted by the solid due to flexing can be modeled with varying levels of complexity. The simplest model is a linear Euler beam theory whereby the pressure jump is $D\,\partial_x^4\zeta$, where ζ is the free surface graph. The flexural rigidity coefficient is $D = \frac{Eh^3}{12(1-\nu^2)}$, where E is the Young's modulus, ν the Poisson ratio and h the thickness of the plate. A nonlinear model often used is the Kirchoff-Love (henceforth denoted as KL) model where the pressure jump is equal to $D\,\partial_x^2\kappa$ where κ is the curvature of the sheet. There are many results for the FG problem with the KL model. Periodic waves were firstly studied by Forbes (1986) and Forbes (1988), and extended to large amplitude by Vanden-Broeck & Părău (2011). Generalized solitary waves were considered by Vanden-Broeck & Părău (2011) in the long wave regime in a fluid of finite depth and

by Milewski *et al* (2011) in the vicinity of the phase speed minimum in deep water. In Părău & Dias (2002), free solitary waves were considered in water of finite-depth. Using the normal form analysis, they found there was a critical depth above which there were no small amplitude solitary waves since the associated nonlinear Schrödinger equation (NLS) was of defocusing type. In other words, free solitary waves bifurcating from infinitesimal periodic waves can only exist in relatively shallow fluids. Most recently, Milewski *et al* (2011) showed that solitary waves also occurred in deep water, but they were of a new type in that they arose along a branch of generalized solitary waves of finite amplitude. These latter two references also considered extensively the *forced* problem modelling a moving load on floating ice.

Although the KL model is widely used in the literature, it does not appear to have an energy formulation. It also does not allow the computation of overhanging waves of large amplitude. Recently, Toland (2008) and Plotnikov & Toland (2011) used the Cosserat theory of hyperelastic shells satisfying Kirchhoff's hypotheses to arrive at a system with variational structure governing the FG problem. In this case, the pressure jump due to bending across the elastic sheet and its corresponding potential energy are of the form

$$D\left(\partial_{ss}\kappa + \frac{1}{2}\kappa^3\right), \qquad \int \kappa^2\, ds \qquad\qquad (1..1)$$

where s is the arc-length. Both this model and the KL model reduce to the Euler beam model for small surface deflections, however this model is expressed in purely geometric terms and therefore does not preclude complex surface shapes. Henceforth in this paper all computations will use this model. Toland (2008) has rigorously proved the existence of FG periodic waves for it and, numerically, Blyth *et al* (2011) studied periodic waves in the absence of gravity. Guyenne & Părău (2012) have computed both depression and elevation solitary waves which exist below the minimum of phase speed at finite amplitude in deep water. Milewski *et al* (2012) have extended the two-dimensional problem modulational analysis to the arbitrary depth three-dimensional problem for all three elastic models. They obtain Benney-Roskes-Davey-Stewartson (BRDS) modulation equations and contrast the three models in the weakly nonlinear regime. Whilst they find that the models are qualitatively similar at small amplitude, this is of course not true for the large amplitude solutions considered in this paper.

In this paper, we study large amplitude FG travelling waves in deep water using the nonlinear elasticity model proposed by Toland (2008). Both periodic and solitary wave bifurcation branches are followed to highly nonlinear regimes. For this model there are both elevation and depression solitary waves (depression waves are waves whose midpoints lie below the mean water level), however in Guyenne & Părău (2012) the branch of elevation waves was not fully explored. Hence, we extend their and show that these waves' branch includes the side-by-side assembly of several depression solitary waves, as a "snaking" bifurcation is traced. For periodic waves, we provide evidence for overhanging waves which ultimately approach a limiting configuration with a free surface profile touching itself at one point.

This paper is structured as follows. In §2, we briefly present a conformal mapping technique used for the steadily travelling potential flow wave problem. In §3, we present the numerical results for solitary waves. Periodic waves, mainly focusing on the overhanging waves, are discussed in §4, and some concluding remarks are presented in §5.

2. Formulation

Consider a train of waves propagating steadily at a constant velocity c on the surface of a two-dimensional fluid of infinite depth and bounded above by an elastic sheet. Introducing cartesian coordinates with

gravity acting in the negative y-direction, and taking a frame of reference moving in the x-direction with the wave results in a steady flow characterised by the velocity $(-c, 0)$ as $y \to -\infty$. The fluid is assumed to be ideal and the flow to be irrotational. We can then introduce a potential function ϕ, such that the fluid velocity field $(u, v) = (-c + \phi_x, \phi_y)$. With the displacement of elastic sheet is designated by $y = \zeta(x)$, the governing equations are

$$
\begin{cases}
\phi_{xx} + \phi_{yy} = 0 & \text{for } -\infty < y < \zeta \\
\phi_x \to -c, \quad \phi_y \to 0 & \text{as } y \to -\infty \\
-(-c + \phi_x)\zeta_x + \phi_y = 0 & \text{at } y = \zeta \\
\frac{1}{2}\left(\phi_x^2 + \phi_y^2\right) - c\phi_x + \zeta + \left(\frac{\kappa^3}{2} + \partial_{ss}\kappa\right) = B & \text{at } y = \zeta
\end{cases}
\tag{2..1}
$$

where $\partial_s = \frac{\partial_x}{\sqrt{1 + \zeta_x^2}}$ in Cartesian coordinates. Here B is the Bernoulli constant. For solitary waves , the flow approaches a uniform stream characterised by a constant velocity $(-c, 0)$ in the far field $x \to \pm\infty$. Choosing $y = 0$ on the free surface in the far field, it follows from the last of the equations (2..1) that $B = \frac{c^2}{2}$. For periodic waves, B can be determined by choosing $y = 0$ as the mean water level, i.e. by imposing

$$
\frac{1}{l} \int_{-l/2}^{l/2} \zeta \, dx = 0
\tag{2..2}
$$

where l is the wavelength. The system (2..1) has been nondimensionalized by choosing

$$
\left(\frac{D}{\rho g}\right)^{1/4}, \qquad \left(\frac{D}{\rho g^5}\right)^{1/8}, \qquad \left(\frac{D^3 g}{\rho^3}\right)^{1/8}
\tag{2..3}
$$

as the units of length, time and potential respectively. Here, ρ is the density of the fluid and g is the acceleration due to gravity.

We shall solve the problem by a boundary integral method. Several approaches have been developed over the years (see Vanden-Broeck (2010) for a review and further references). Here we follow the approach used by Dyachenko *et al* (1996) and later by Milewski *et al* (2012) for the FG problem. The main idea is to conformally map the physical domain into the lower half-plane of a new complex plane whose horizontal and vertical coordinates will be denoted by ξ and η. The map itself can be defined as the solution of the boundary value problem

$$
\begin{cases}
y_{\xi\xi} + y_{\eta\eta} = 0 & \text{for } -\infty < \eta < 0 \\
y = Y(\xi, \eta) & \text{at } \eta = 0 \\
y \sim \eta & \text{as } \eta \to -\infty
\end{cases}
\tag{2..4}
$$

where $Y(\xi) = \zeta(x(\xi, 0))$. The harmonic conjugate variable $x(\xi, \eta)$ is defined through the Cauchy-Riemann relations for the analytic function $z(\xi, \eta) = x(\xi, \eta) + iy(\xi, \eta)$. In the transformed plane, we define $X(\xi) \triangleq x(\xi, 0)$, $\Phi(\xi) \triangleq \phi(\xi, 0)$ and $\Psi(\xi) \triangleq \psi(\xi, 0)$, where ψ is the harmonic conjugate of the potential ϕ. From elementary harmonic analysis one obtains

$$
\Phi_\xi = -\mathscr{H}[\Psi_\xi], \qquad X = \xi - \mathscr{H}[Y]
\tag{2..5}
$$

where $\mathscr{H}$ is the Hilbert transform with the Fourier symbol $i\,sgn(k)$, i.e.,

$$\mathscr{H}[f] \;=\; \mathscr{F}^{-1}\big[i\,sgn(k)\mathscr{F}[f]\big]. \tag{2..6}$$

where $\mathscr{F}$ is the Fourier transform and $\mathscr{F}^{-1}$ is its inverse. By application of the relation (2..5) and chain rule, the kinematic boundary condition is reduced to the simple expression $\Psi_\xi = 0$ (i.e. the stream function is constant on the free surface), and the dynamic boundary condition to

$$\frac{c^2}{2J} + Y + \mathscr{M} = B \tag{2..7}$$

where $J \triangleq X_\xi^2 + Y_\xi^2$ and $\mathscr{M}$ takes the form

$$\mathscr{M} = \frac{\kappa_{xx}}{1+\zeta_x^2} - \frac{\zeta_x\zeta_{xx}\kappa_x}{(1+\zeta^2)^2} + \frac{\kappa^3}{2} = \frac{1}{2}\left[\frac{\kappa_{\xi\xi}}{J} + \left(\frac{\kappa_\xi}{J}\right)_\xi + \kappa^3\right] \tag{2..8}$$

and

$$\kappa = \frac{X_\xi Y_{\xi\xi} - X_{\xi\xi}Y_\xi}{J^{3/2}} \tag{2..9}$$

Equation (2..7) together with $X_\xi = 1 - \mathscr{H}[Y_\xi]$, completes the formulation as a system of integro-differential equations. The unknowns are solving c and Y in the case of solitary waves. For periodic waves, we take B as an unknown and (2..2) needs to be satisfied. In all computations, the waves are assumed to be symmetric with respect to $x = 0$. The nonlinear algebraic-differential equation (2..7) is solved using a collocation method with a set of cosine basis functions whose coefficients are solved with Newton's method. That is, we set

$$Y(\xi) = \sum_{j=1}^{N} a_j \cos\left(j\pi\xi/L\right)$$

with the a_j as unknowns to be solved through Newton iteration. The equation (2..7) is evaluated on uniform grid points in $[0,L]$ with the Hilbert transform and derivatives obtained by using the Fourier multipliers, while the nonlinear terms are computed in the physical space. For solitary waves the period L is chosen sufficiently large such that the solution does not change when L is further increased whilst for periodic waves we choose $L = \pi$ (see Section 4.). N is also chosen sufficiently large so that the solution no longer changes if N is increased. The method was used successfully in Milewski et al (2012).

3. Solitary Waves

Some insight into the problem can be gained by first considering linear periodic waves. The equations (2..1) have the exact "trivial" solution $\phi = -cx$, $\zeta = 0$ which corresponds to a uniform stream. Writing $\phi = -cx + \varphi$ and linearising (2..1) by assuming that $|\varphi|$ and $|\zeta|$ are small leads to periodic waves with speed given by the dispersion relation (see for example Squire et al (1996) for details)

$$c^2 \;=\; \frac{1}{k} + k^3 \tag{3..1}$$

where c is the phase speed and k the wavenumber.

The phase speed has a global minimum $c = c^*$ for $k = k^*$ where

$$k^* = \left(\frac{1}{3}\right)^{1/4} \approx 0.7598, \qquad c^* = \sqrt{3^{\frac{1}{4}} + 3^{-\frac{3}{4}}} \approx 1.3247 \tag{3..2}$$

Whilst periodic nonlinear waves can bifurcate from any k, solitary waves bifurcate generically from particular k corresponding to extrema of phase speed. There, the group speed is equal to the phase speed, a necessary condition for the existence of weakly nonlinear solitary waves. If the extremum occurs at finite k, the solitary waves will generally have decaying oscillatory tails. Whether or not solitary waves bifurcate from a finite k extremum can be decided using normal form analysis. Assuming $\zeta = \varepsilon A(\varepsilon x)\, e^{ik^*x} + c.c. + o(\varepsilon)$, $c = c^* + \varepsilon^2 C + o(\varepsilon^2)$, where ε is a small parameter, one can show that the envelope of the carrier oscillation is governed by the steady cubic nonlinear Schrödinger equation (NLS)

$$k^*CA + \frac{3^{7/8}}{2}A_{XX} = \frac{1}{44} \cdot 3^{-9/8}|A|^2A \tag{3..3}$$

The derivation is well known, so we omit the details here. It can be found in Părău & Dias (2002), and a more complete derivation of the time dependent NLS equation can be found in Guyenne & Părău (2012) or Milewski *et al* (2011). Since (3..3) does not support localised solution (i.e. the corresponding time-dependent NLS is defocusing) it predicts the non-existence of small amplitude solitary waves. Nevertheless, Milewski *et al* (2011) and Guyenne & Părău (2012) found solitary waves with *finite* amplitude and $c < c^*$ for the full potential system (2..1).

The amplitude-speed bifurcation diagram for both elevation and depression solitary waves are shown in Figure 1. The depression branch mostly reproduces the result of Guyenne & Părău (2012) (although we extend the branch continuously to $c = 0$). It is clear from the figure that both branches start at finite amplitudes for $c = c^* \approx 1.3247$. This is different from the well-known case of gravity-capillary solitary waves which bifurcate from a train of infinitesimal periodic waves (see Vanden-Broeck (2010) for a review). Typical profiles of the depression solitary wave are shown in Figure 2. As in Guyenne & Părău (2012) we find that as the speed c decreases, the depression solitary waves become steeper, eventually with an overhanging profiles. Further down the curve the profile develops a point of contact with a "trapped bubble" at the trough. For even smaller values of c the profiles become self-intersecting which is nonphysical, but mathematically well-defined. Solutions can be computed for all values of c down to a static state $c = 0$ at which point there is no flow and the only fluid effect is hydrostatic pressure. (Of course, the solution branch continues symmetrically for c negative.) A similar trapped bubble structure has also been found in capillary-gravity waves by Vanden-Broeck & Dias (1992). In all the computations of Figure 2, 2048 Fourier modes were used and the physical domain size is changed appropriately for the sake of accuracy depending on the decay of the solution.

The branch of elevation solitary waves, which was not explored fully in Guyenne & Părău (2012), is far more complicated. The detail of the amplitude-speed bifurcation diagram are shown in Figure 3, and same curve on energy-speed axes are shown in Figure 5. The energy of steady solitary waves is given by

$$\text{Energy} = -\frac{c}{2}\int Y d\xi + \frac{1}{2}\int Y^2 X_\xi d\xi + \frac{1}{2}\int \frac{(Y_{\xi\xi}X_\xi - X_{\xi\xi}Y_\xi)^2}{J^{5/2}}d\xi. \tag{3..4}$$

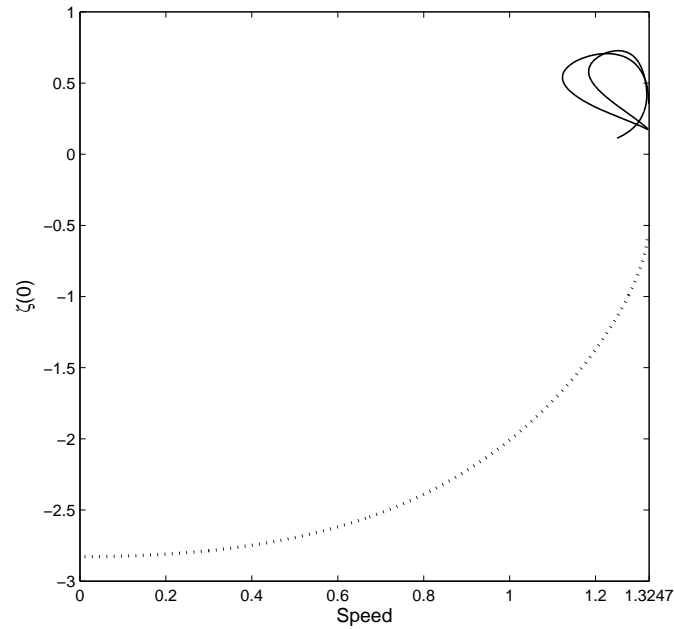　　　　　Z. Wang, J.-M. Vanden-Broeck & P. A. Milewski

FIG. 1. Elevation (solid curve) and depression (dashed curve) branches of solitary wave solutions. More detail of the elevation wave branch is shown in Figure 3.
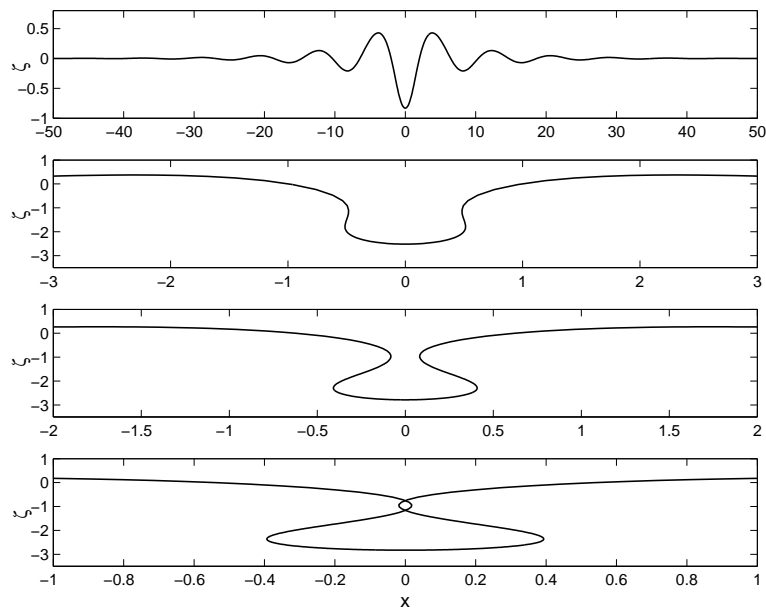

FIG. 2. Free-surface profiles of depression solitary waves, from c near the bifurcation point $c*$ (top) to the static state $c = 0$ (bottom). From top to bottom: $c = 1.3$, $c = 0.7$, $c = 0.3$, $c = 0$. Only part of the horizontal domain is shown.
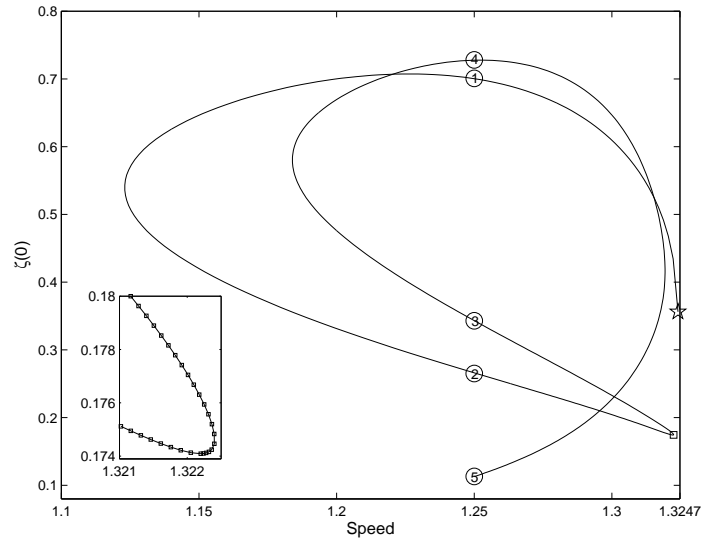
FIG. 3. The "snaking" bifurcation of the elevation branch of solitary waves. Starting from the 'star' and following the path ① → ② → ③ → ④ → ⑤. The waves corresponding to the circled numbers have the same propagation speed $c = 1.25$ and the profiles are shown in Figure 5. There is a turning point between every two adjacent circled numbers. The sharp nature of the second turning point (labeled as a 'square') is shown in more detail.

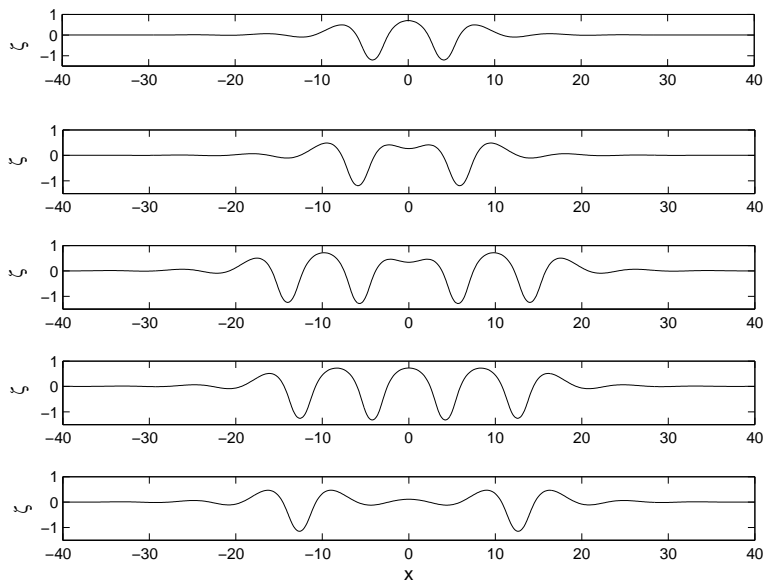FIG. 4. Typical profiles of the elevation solitary waves at speed $c = 1.25$. From top to bottom, the profiles correspond to ① − ⑤ labeled in Figure 3 respectively.
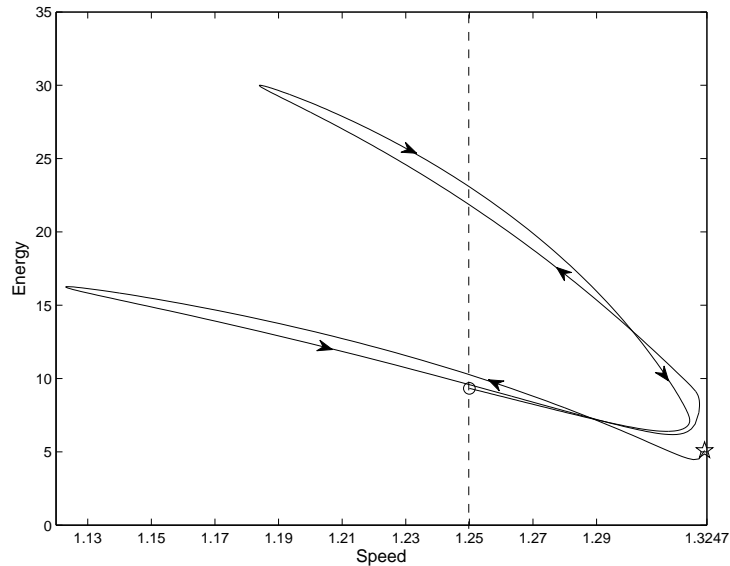
Z. Wang, J.-M. Vanden-Broeck & P. A. Milewski

FIG. 5. Energy-speed bifurcation diagram of elevation solitary waves. The curve begins from the star and is computed up to the circle. The path has been labeled with arrows. The dashed line represents the translating speed $c = 1.25$, and the intersection points with solid curve correspond to the circled numbers ① − ⑤ in Figure 3.

The curves exhibit multiple turning points. Such multiple turning points have also been found in the bifurcation diagram of the elevation capillary-gravity solitary waves by Dias *et al* (1996). The profiles corresponding to the labelled points on the curves are shown in Figure 4. The elevation wave numerical computations required a large number of Fourier modes (typically 8192) and domain size (typically L=400) since the solitary waves can be very broad. The computations were stopped after passing through the forth turning point when two almost completely separated depression solitary waves appear. At this point the solution becomes very sensitive (presumably since the waves are far apart their separation is sensitive to perturbations) and more accurate computations became prohibitive. At turning points the parameter along the curve had to be changed, and we alternated between using $\zeta(0)$ and c in order to complete the curve.

From the profiles in Figure 4 and the corresponding energy bifurcation diagram in Figure 5, one sees that the solutions either have two or four main troughs. Along each "arm" of the energy bifurcation figure the number of troughs doesn't change and the separation distance between the troughs is the main qualitative change in the solutions. The profiles ③ and ④ have approximately twice the energy of ① ② and ⑤ since they have double the number of similar amplitude troughs.

4. Periodic Waves

In this section we use the nonlinear elasticity model of Toland (2008) to calculate weakly nonlinear and fully nonlinear solutions for periodic waves. Such results were previously computed by Vanden-Broeck & Părău (2011) for the KL model. For simplicity we assume that the water is of infinite depth. Solutions

for weakly nonlinear periodic waves can be constructed analytically by using a Stokes expansion, i.e. an asymptotic expansion in powers of the wave amplitude. Wilton (1915) used the Stokes expansion to study capillary-gravity waves and his results showed that, in contrast to pure gravity waves, there may be many families of solutions with a given base period.

To construct "Wilton ripples", we introduce a small parameter ε which is a measure of the amplitude of the wave, so that the wave reduces to a uniform stream as $\varepsilon \to 0$ and write the expansions

$$
\begin{aligned}
\phi &= cx + \varepsilon\phi_1 + \varepsilon^2\phi_2 + \varepsilon^3\phi_3 + \cdots \\
\zeta &= \varepsilon\zeta_1 + \varepsilon^2\zeta_2 + \varepsilon^3\zeta_3 + \cdots \\
c &= c_0 + \varepsilon c_1 + \varepsilon^2 c_2 + \varepsilon^3 c_3 + \cdots \\
B &= B_0 + \varepsilon B_1 + \varepsilon^2 B_2 + \varepsilon^3 B_3 + \cdots
\end{aligned}
$$

Substituting this ansatz into the system (2..1) and equating powers of ε lead to a succession of linear systems. These linear systems can be solved, although the amount of algebra increases rapidly as the order increases. At leading order,

$$
\zeta_1(x) = \cos kx \tag{4..1}
$$

$$
\phi_1(x,y) = c_0 e^{ky} \sin kx \tag{4..2}
$$

$$
c_0^2 = \frac{1}{k} + k^3 \tag{4..3}
$$

The definition of ε is such that the coefficient of $\cos kx$ in (4..1) is 1. The leading order solution (4..1)-(4..3) is the solution to the linearized problem and (4..3) is the dispersion relation (3..1). It has a global minimum defined by (3..2) and there are particular values of k for which linear waves of wavenumbers k and mk travel at the same speed. If $m \geqslant 2$ is an integer these waves can be used to construct other solutions with the same period as (4..1). To see this, write

$$
c_0^2 = \frac{1}{k} + k^3 = \frac{1}{mk} + (mk)^3 \tag{4..4}
$$

and solve for k. This leads to

$$
k = \left[\frac{1}{m(m^2 + m + 1)} \right]^{1/4} \tag{4..5}
$$

Therefore when (4..5) is satisfied the solutions (4..1) and (4..2) need to be replaced by

$$
\zeta_1(x) = \cos kx + A_m \cos mkx \tag{4..6}
$$

$$
\phi_1(x,y) = c_0 e^{ky} \sin kx + A_m c_0 e^{mky} \sin mkx \tag{4..7}
$$

where A_m is a constant. The value of A_m is then found at higher order in the expansions in power of ε. The existence of many families of solution comes from the fact that the value of A_m is not unique. For example calculating solutions up to second order shows that $A_2 = \pm\frac{1}{2}$. The details of the calculations are identical to those presented by Vanden-Broeck & Părău (2011) for the KL model since the two models agree up to second order. For $m > 2$, it is necessary to go to higher order to impose the solvability condition for A_m and the Wilton ripples no longer agree even at small amplitude. Figure **??** shows typical $m = 3$ profiles. Clearly, at large amplitudes, such profiles also have overturning points.

Lastly we consider the limiting configuration of very steep periodic waves. In the fully nonlinear regime, overhanging profiles are typical in water wave problems in the presence of additional surface
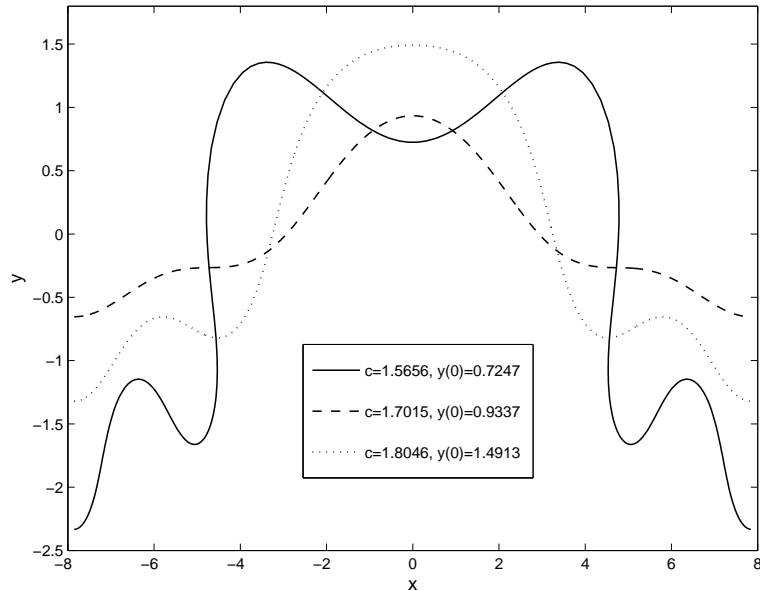
FIG. 6. Typical profiles of large amplitude Wilton-like periodic flexural-gravity waves for $m = 3$. Note that one of the profiles is overhanging.

effects such as surface tension. This has been found analytically for pure capillary waves (Crapper (1957)) and computed numerically for capillary-gravity periodic waves (see Vanden-Broeck (2010) for a review). Furthermore, these overhanging waves ultimately approach limiting configurations in which the free surface touches itself at one point forming a "trapped bubble". Forbes (1988) suggested that overhanging waves should also occur in the FG problem. This was confirmed numerically by Vanden-Broeck & Părău (2011) using the KL model, however, due to numerical difficulties, the computations had to be stopped much before a profile with a trapped bubble was reached. Overhanging waves up to the configuration with a trapped bubble, and beyond that, unphysical self-intersecting profiles, can easily be computed when the nonlinear elastic model of Toland (2008) is used.

As an example of our numerical experiments, we chose 2π as the wavelength to avoid the critical values (4..5). The results are presented in Figure 7, and were obtained with 512 grid points (256 Fourier modes) and $\Delta\xi \approx 0.012$, and are unchanged within graphical accuracy when the number of grid points is increased. As propagating speed c decreases, the periodic waves demonstrate overhanging structure, and finally reach static configurations corresponding to $c = 0$ where the only hydrodynamic effect is the hydrostatic pressure. The self-intersecting structure in the static state has been partially enlarged in the bottom graph for clarity.

5. Conclusions

An efficient numerical procedure to compute nonlinear steady flexural-gravity free-surface flows is implemented. The flow is assumed to be potential and a simple conservative nonlinear elastic model is used to model the floating structure. Solitary and periodic waves are computed. New elevation solitary waves are found. These complement the results of Guyenne & Părău (2012). For periodic waves, the
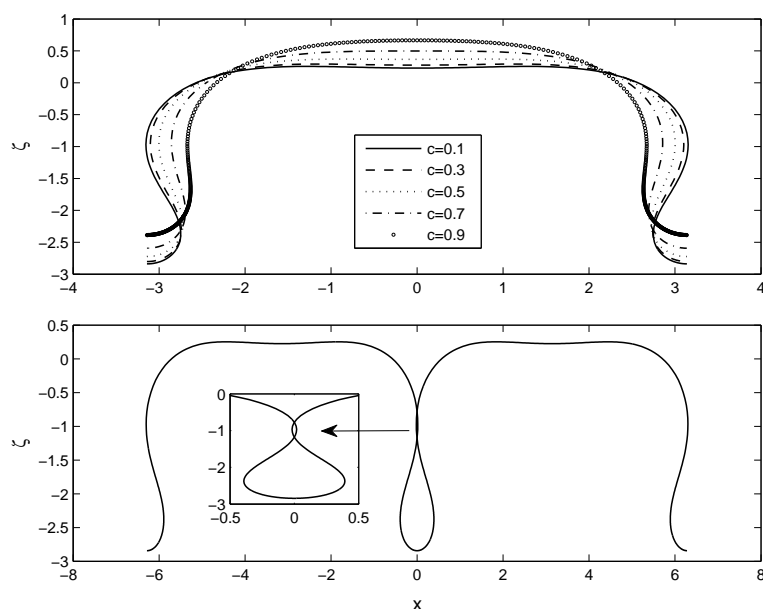
FIG. 7. Typical profiles of overhanging structure in periodic flexural-gravity waves. Top: profiles with different propagating speed, $c = 0.9$ (circles), $c = 0.7$ (dot-dashed curve), $c = 0.5$ (dotted curve), $c = 0.3$ (dashed curve) and $c = 0.1$ (solid curve). Bottom: the periodic waves reach 'limiting' configuration corresponding to the static state.

present elastic model enables the computation of overhanging waves even beyond the limiting configuration where the free surface touches itself at one point. Whilst it is beyond the scope of this paper, we believe that the stability problem for both branches of solitary waves could be particularly interesting.

References

BLYTH, M. G., PĂRĂU, E. I. & VANDEN-BROECK, J.-M. (2011) Hydroelastic waves on fluid sheets, *J. Fluid Mech.*, **689**, 541–551.

CRAPPER, G. D. (1957) An exact solution for progressive capillary waves of arbitrary amplitude, *J. Fluid Mech.*, **2**, 532–540.

DIAS, F., MENASCE, D. & VANDEN-BROECK, J.-M. (1996) Numercial study of capillary-gravity solitary waves, *Eur. J. Mech., B/Fluid*, **15(1)**, 17–36.

DYACHENKO, A. I., KUZNETSOV, E. A., SPECTOR, M. D. & ZAKHAROV, V. E. (1996) Analytical description of the free surface dynamics of an ideal fluid (canonical formalism and conformal mapping), *Phys. Lett. A*, **221**, 73–79.

FORBES, L. K. (1986) Surface waves of large amplitude beneath an elastic sheet. I. High-order series solution, *J. Fluid Mech.*, **169**, 409–428.

FORBES, L. K. (1988) Surface waves of large amplitude beneath an elastic sheet. II. Galerkin solution, *J. Fluid Mech.*, **188**, 491–508.

GUYENNE, P. & PĂRĂU, E. I. (2012) Computations of fully nonlinear hydroelastic solitary wave on deep water, *J. Fluid Mech.*, in press.

HEGARTY, G. M. & SQUIRE, V. A. (2002) Large amplitude periodic waves beneath an ice sheet. In *Ice in the Environment. Proc. 16th IAHR Int. Symp. on Ice*, vol.2 (eds V.A. Squire & P.J. Langhorne), 310–317, Madrid, Spain: International Association of Hydraulic Engineering and Research.

MILEWSKI, P. A., VANDEN-BROECK, J.-M. & WANG, Z. (2011) Hydroelastic solitary waves in deep water, *J. Fluid Mech.*, **679**, 628–640.

MILEWSKI, P. A., VANDEN-BROECK, J.-M. & WANG, Z. (2012) Steady dark solitary flexural gravity waves, *Proc. R. Soc. A*, in press.

MILEWSKI, P. A. & WANG, Z. (2012) Three dimensional flexural-gravity waves, *Studies in Appl. Math.*, to appear.

PĂRĂU, E. I. & DIAS, F. (2002) Nonlinear effects in the response of a floating ice plate to a moving load, *J. Fluid Mech.*, **460**, 281–305.

PLOTNIKOV, P. I. & TOLAND, J. F. (2011) Modelling nonlinear hydroelastic waves, *Phil. Trans. R. Soc. Lond. A*, **369**, 2942–2956.

SQUIRE, V. A., HOSKING, R. J., KERR, A. D. & LANGHORNE, P. J. (1996) Moving Loads on Ice Plates (Solid Mechanics and Its Applications), Kluwer.

TOLAND, J. F. (2008) Steady periodic hydroelastic waves, *Arch. Ration. Mech. Anal.*, **189(2)**, 325–362.

VANDEN-BROECK, J.-M. (2010) Gravity-capillary free-surface flows. Cambridge, UK: Cambridge University Press.

VANDEN-BROECK, J.-M. & DIAS, F. (1992) Gravity-capillary solitary waves in water of infinite depth and related free-surface flows, *J. Fluid Mech.*, **240**, 549–557.

VANDEN-BROECK, J.-M. & PĂRĂU, E. I. (2011) Two-dimensional generalized solitary waves and periodic waves under an ice sheet, *Phil. Trans. R. Soc. Lond. A*, **369**, 2957–2972.

WILSON, J. T.(1958) Moving loads on floating ice sheets. University of Michigan Research Institute (UMRI Project 2432).

WILTON, J. R. (1915) On ripples, *Phil. Mag.*, **29**, 688–700.